Clim Dyn (2017) 49:3799–3811
DOI 10.1007/s00382-017-3544-x

A possible explanation for the divergent projection of ENSO amplitude change under global warming

Lin Chen[1,2,3,4] · Tim Li[1,2] · Yongqiang Yu[3,4] · Swadhin K. Behera[5]

Received: 6 August 2016 / Accepted: 18 January 2017 / Published online: 26 February 2017

Abstract The El Niño-Southern Oscillation (ENSO) is the greatest climate variability on interannual time scale, yet what controls ENSO amplitude changes under global warming (GW) is uncertain. Here we show that the fundamental factor that controls the divergent projections of ENSO amplitude change within 20 coupled general circulation models that participated in the Coupled Model Intercomparison Project phase-5 is the change of climatologic mean Pacific subtropical cell (STC), whose strength determines the meridional structure of ENSO perturbations and thus the anomalous thermocline response to the wind forcing. The change of the thermocline response is a key factor regulating the strength of Bjerknes thermocline and zonal advective feedbacks, which ultimately lead to the divergent changes in ENSO amplitude. Furthermore, by forcing an ocean general circulation mode with the change of zonal mean zonal wind stress estimated by a simple theoretical model, a weakening of the STC in future is obtained. Such a change implies that ENSO variability might strengthen under GW, which could have a profound socio-economic consequence.

Keywords ENSO · Global warming · Ocean thermocline response to wind anomaly · ENSO meridional structure · Subtropical cell

✉ Tim Li
timli@hawaii.edu

[1] Key Laboratory of Meteorological Disaster, Ministry of Education (KLME)/Joint International Research Laboratory of Climate and Environmental Change (ILCEC)/ Collaborative Innovation Center on Forecast and Evaluation of Meteorological Disasters (CIC-FEMD), Nanjing University of Information Science and Technology, Nanjing, China

[2] International Pacific Research Center (IPRC), and Department of Atmospheric Sciences, SOEST, University of Hawaii at Manoa, Honolulu, HI 96822, USA

[3] State Key Laboratory of Numerical Modeling for Atmospheric Sciences and Geophysical Fluid Dynamics (LASG), Institute of Atmospheric Physics (IAP), Chinese Academy of Sciences (CAS), Beijing 100029, China

[4] College of Earth Science, University of Chinese Academy of Sciences, Beijing, China

[5] Application Laboratory, Japan Agency for Marine-Earth Science and Technology, Yokohama, Japan

1 Introduction

As the greatest natural climate variability on interannual timescale, ENSO exerts pronounced influences on climate and weather around the globe (Philander 1990; Ding and Li 2012; Feng and Li 2011, 2013; Karori et al. 2013; Zhang et al. 2013a). ENSO itself is known to have complicated variations under different backgrounds. For instance, more frequent central Pacific El Niño (CP El Niño) events is observed after 2000s, which may be due to global warming (hereafter GW) (e.g., Yeh et al. 2009) or due to the interdecadal mean state change (e.g., Chung and Li 2013; Xiang et al. 2013). The new type of El Niño (Larkin and Harrison 2005; Ashok et al. 2007; Kao and Yu 2009; Kug et al. 2009) was reported to exert a distinctive climate impact (e.g., Feng and Li 2011, 2013; Xiang et al. 2013; Feng et al. 2016) compared to the traditional eastern Pacific El Niño. Thus, understanding the changes of ENSO behaviors is the first step to figure out its varying influence on Earth's climate system (McPhaden et al. 2006; Collins et al. 2010).

Under the continued anthropogenic greenhouse forcing, how the ENSO variability might vary has been a hot debating topic, yet there is no consensus in projected ENSO

amplitude changes in recent reports (e.g., Zelle et al. 2005; Van Oldenborgh et al. 2005; Merryfield 2006; DiNezio et al. 2009; Yeh and Kirtman 2007; Latif and Keenlyside 2009; Stevenson 2012; Power et al. 2013; Cai et al. 2015a; Kim et al. 2014). For example, by employing a coupled model with a large number of ensemble members, Zelle et al. (2005) found no apparent changes in ENSO amplitude as a response to increasing greenhouse gases. Some previous work (e.g., Van Oldenborgh et al. 2005; Merryfield 2006; Guilyardi 2009; Latif and Keenlyside 2009; Collins et al. 2010) pointed out that there is no consistency in the projected ENSO amplitude change under GW, through analyzing the multi-model simulations from Coupled Model Intercomparison Project (CMIP) phase-3 (CMIP3).

We examined the response of ENSO amplitude to the scenario of GW, using outputs from the latest CGCMs in CMIP phase-5 (CMIP5). A divergent projection of future ENSO amplitude changes is clearly seen in Fig. 1a. Our result shows that among the 20 CMIP5 models, six models with strengthened ENSO amplitude and eight models with weakened amplitude pass the statistically significance of F-test (marked by a red or blue check in Fig. 1a). The divergent ENSO projections raise a fundamental question, namely, what are fundamental processes controlling ENSO amplitude changes under GW in CMIP5 models?

Several recent studies have devoted efforts into addressing this issue. Kim et al. (2014) suggested the ENSO intensity change is tied to the change of mean zonal thermocline slope and mean zonal SST contrast, via analyzing the simulations in nine better CGCMs selected from CMIP5. Through concentrating on the atmospheric feedbacks, Rashid et al. (2016) suggested the difference in the zonal wind stress forcing efficiency is a possible cause for the contrasting ENSO amplitude changes. Chen et al. (2015) argued that the ENSO amplitude change is associated with the change of the climatological subtropical cell (STC). But their analysis is based on only four CMIP5 models. Additionally, Ham and Kug (2016) proposed that the ENSO amplitude change is linked with the atmospheric mean state change in present-day simulation, that is, stronger positive tropical precipitation change may cause strengthened ENSO variability.

Motivated by complex possible factors contributing to divergent projection of ENSO amplitude change, in this study we intend to adopt a step-by-step approach to investigate the factors controlling the divergent ENSO amplitude change in CMIP5 models. For example, because ENSO development undergoes various positive and negative feedback processes (Li 1997), such as the Bjerknes SST-wind-thermocline feedback (hereafter TH feedback), zonal advective feedback (hereafter ZA feedback) and anomalous upwelling feedback, it's necessary to first investigate what feedback processes are critical for explaining the divergent ENSO amplitude change. Given that the change of

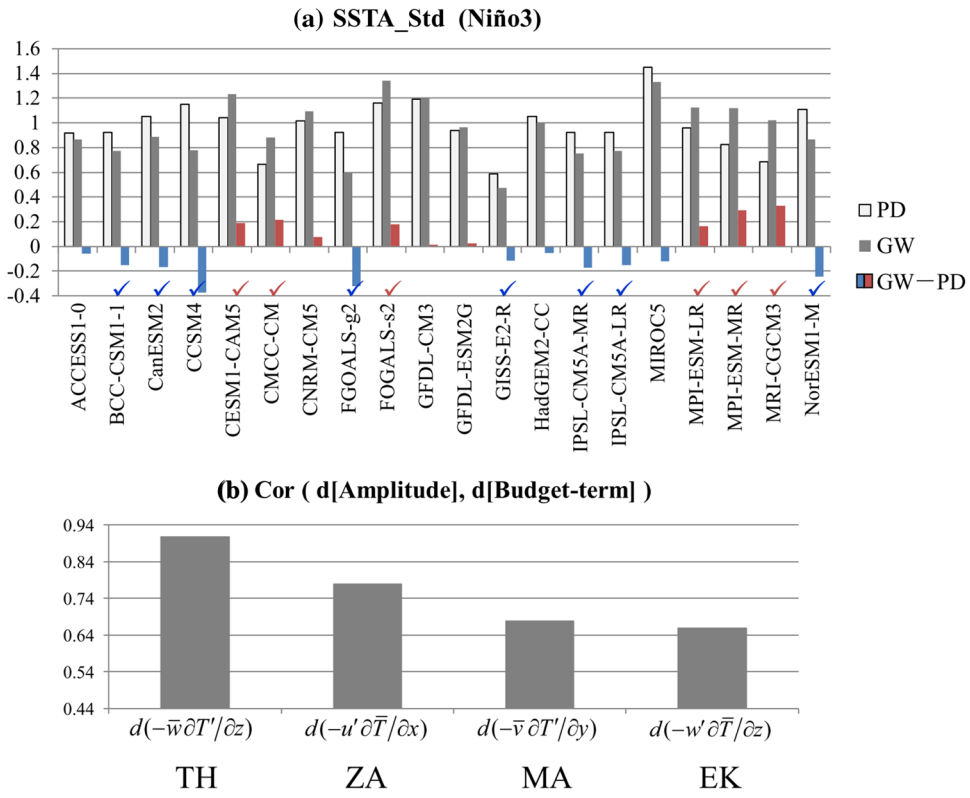

Fig. 1 **a** The changes in the standard deviation (STD) of sea surface temperature anomaly (SSTA) over Niño3 region from PD (historical experiment) to GW (RCP8.5 experiment) (GW minus PD; unit: K) derived from 20 CMIP5 models. The *red* (*blue*) *check mark* indicates the strengthened (weakened) model, whose ENSO amplitude change exceeding the 95% confidence level based on the F-test. **b** The correlations between ENSO amplitude change and the change in the four leading budget terms. The significance at 95% confidence level is 0.44 using a *t* test

ENSO-related feedbacks involves both the ENSO perturbation change and mean state change, it's important to illustrate the relative role of the perturbation change and mean state change. Through this step-by-step approach, the main purpose of this work is to reveal the key factors controlling the ENSO amplitude change under GW in CMIP5 models.

In Sect. 2, the primary data and methods are introduced. Section 3 presents the dominant air-sea feedback processes determining the divergent changes in the ENSO amplitude under GW. In Sect. 4, we investigated what causes of distinctive thermocline response change under GW. In Sect. 5, the cause of ENSO meridional structure changes is analyzed. In Sect. 6, we further discussed how the mean STC would change under GW. In Sect. 7, we will give the summary and discussion.

2 Data and methods

Twenty CMIP5 (Taylor et al. 2012) model outputs were utilized in this study. The historical run for the period of 1951–2005 is used as the present-day (PD) simulation and the RCP8.5 run for the period of 2051–2100 is used as future projection simulation under GW. Interannual anomaly fields are obtained by first de-trending original datasets and then removing the model climatologic annual cycle.

To investigate the relative roles of thermodynamic and dynamic processes in causing different tendencies of sea surface temperature anomaly (SSTA) during the ENSO development, the mixed-layer heat budget was diagnosed based on the equation of temperature tendency (Li et al. 2002; Chen et al. 2015):

$$\begin{aligned}\partial T'/\partial t = &-u'\partial\overline{T}/\partial x - \overline{u}\partial T'/\partial x - u'\partial T'/\partial x - w'\partial\overline{T}/\partial z \\ &- \overline{w}\partial T'\partial z - w'\partial T'/\partial z - v'\partial\overline{T}/\partial y \\ &- \overline{v}\partial T'/\partial y - v'\partial T'/\partial y + \frac{Q'_{net}}{\rho_0 C_p H} + R\end{aligned} \tag{1}$$

where u, v, w and T are the 3-D oceanic current and temperature; a prime indicates the interannual anomaly field; a bar indicates the climatologic mean field; Q_{net} indicates the net surface heat flux (the positive sign represents that the ocean receives heat); R indicates the residuals; C_p and ρ_0 are, respectively, the specific heat of seawater and the density of seawater; and H represents the mixed-layer depth, which is defined as the depth where ocean temperature is 0.5 °C lower than the surface and varies with time and space.

To explore the cause of anomalous zonal ocean current, the anomalous zonal geostrophic and Ekman currents were diagnosed. According to previous studies (Chang and Philander 1994; Wang and Weisberg 1994; Su et al. 2010), the anomalous zonal geostrophic current (u_g') and the anomalous zonal Ekman current (u_e') may be written as

$$u'_g = -\frac{g\partial^2 D'}{\beta\partial y^2}, \tag{2}$$

$$u'_e = \frac{1}{\rho H}\frac{r_s\tau'_x + \beta y\tau'_y}{\tau_s^2 + (\beta y)^2}, \tag{3}$$

in which D' represents the anomalous thermocline depth; g and β denote, respectively, the meridional gradient of planetary vorticity and the reduced gravity; r_s denotes the coefficient of Rayleigh damping; τ_x' (τ_y') denotes the wind stress anomaly in zonal (meridional) direction.

The ocean general circulation mode (OGCM) used in this study is LICOM2.0 (for details, see Liu et al. 2012). LICOM2.0 is the ocean component of the coupled general circulation models of both FGOALS-s2 and FGOALS-g2, which have participated in CMIP5. In the control run, LICOM2.0 was driven by the climatological wind stress and heat flux from ERA40. After reaching a quasi-equilibrium state, the last 40 years of integration is used for climatology analysis. In the sensitivity experiment, the forcing field of wind stress is replaced by the summation of ERA40 climatology and the theoretically estimated change of mean zonal wind stress, while the other forcing fields keep unchanged as the control run. Through analyzing the difference of mean meridional current/STC between control run and sensitivity experiment, one may investigate the influence of the mean zonal wind stress change on the mean STC change.

3 Dominant air-sea feedback processes for divergent ENSO amplitude changes under GW

3.1 Mixed-layer heat budget

A mixed-layer heat budget analysis was performed for composite ENSO events during the ENSO developing phase for both the PD and GW simulations in each of 20 CMIP5 models. The result shows that the dominant feedback processes that control the ENSO amplitude change are, in a rank from the highest to the lowest (all of which pass 95% significance level based on t-test), the TH feedback ($-\bar{w}\frac{\partial T'}{\partial z}$), ZA feedback ($-u'\frac{\partial\overline{T}}{\partial x}$), meridional advection feedback ($-\bar{v}\frac{\partial T'}{\partial y}$; hereafter MA feedback), and Ekman pumping induced anomalous upwelling feedback ($-w'\frac{\partial\overline{T}}{\partial z}$; hereafter EK feedback) (Fig. 1b). Note that in the heat budget analysis above, all dynamic (three-dimensional advection) and

thermodynamic (heat flux) terms are calculated, and only the four heat budget terms that have positive correlations exceeding the 95% confidence are analyzed here. Both the correlation coefficients and the actual values of the budget terms indicate that the four feedback processes mentioned above make the most important contributions to divergent ENSO amplitude changes.

3.2 Analysis of thermocline feedback change

Among the changes in the aforementioned four feedback terms, the change in the TH feedback term is most critical (Figs. 1b, 2a). Thus, to figure out the dynamics of the change of ENSO amplitude under GW, it's necessary to explore what causes the changes in the TH feedback term. The growth-rate related to the TH feedback term $(-\bar{w}\frac{\partial T'}{\partial z})$ could be expressed in the following way (Liu et al. 2011; Chen et al. 2015):

$$\sigma = \frac{\overline{w}}{H} R(\tau_x^{'}, T^{'}) R(D^{'}, \tau_x^{'}) R(T_e^{'}, D^{'}), \tag{4}$$

where σ represents the growth-rate, $\bar{w}$ represents the climatologic mean vertical upwelling velocity, H represents the oceanic mixed-layer depth, τ_x' denotes zonal wind stress anomaly, $D^{'}$ represents the thermocline depth anomaly, T' denotes SSTA and T'_e represents the oceanic temperature anomaly in subsurface. Equation (4) suggests that besides the climatological upwelling velocity, the ENSO growth rate related to TH feedback is determined by three feedback coefficients: $R(\tau_x', T')$representing how the τ_x' over the central equatorial Pacific (CEP) would change in response to the SSTA over the equatorial eastern Pacific (EEP), $R(D', \tau_x')$ representing the effect of a unit τ_x' over CEP on the change of $D^{'}$ over EEP, $R(T_e', D')$ representing how the oceanic subsurface temperature over EEP would change in response to a unit D' over EEP.

Note that all the aforementioned four feedback terms are the product of a perturbation part and a mean state part. For example, the TH feedback term is a product of $-\frac{\partial T'}{\partial z}$ and $\bar{w}$. Because both the perturbation part and the mean state part may change under GW, it is of importance to identify the relative contribution of perturbation change and mean state change to the change of the feedback terms. According to the total differential relationship, Chen et al. (2015) separated the contributions from mean state change and perturbation change, and pointed out that the change of ENSO perturbation is essential in the change of the four major budget terms, while the direct influence from the equatorial mean state change is minor. Consistent with this result, the change of the TH feedback term associated with the growth rate in Eq. (4) is negatively correlated with the change of the mean vertical velocity ($\bar{w}$), as shown in Fig. 2b. This

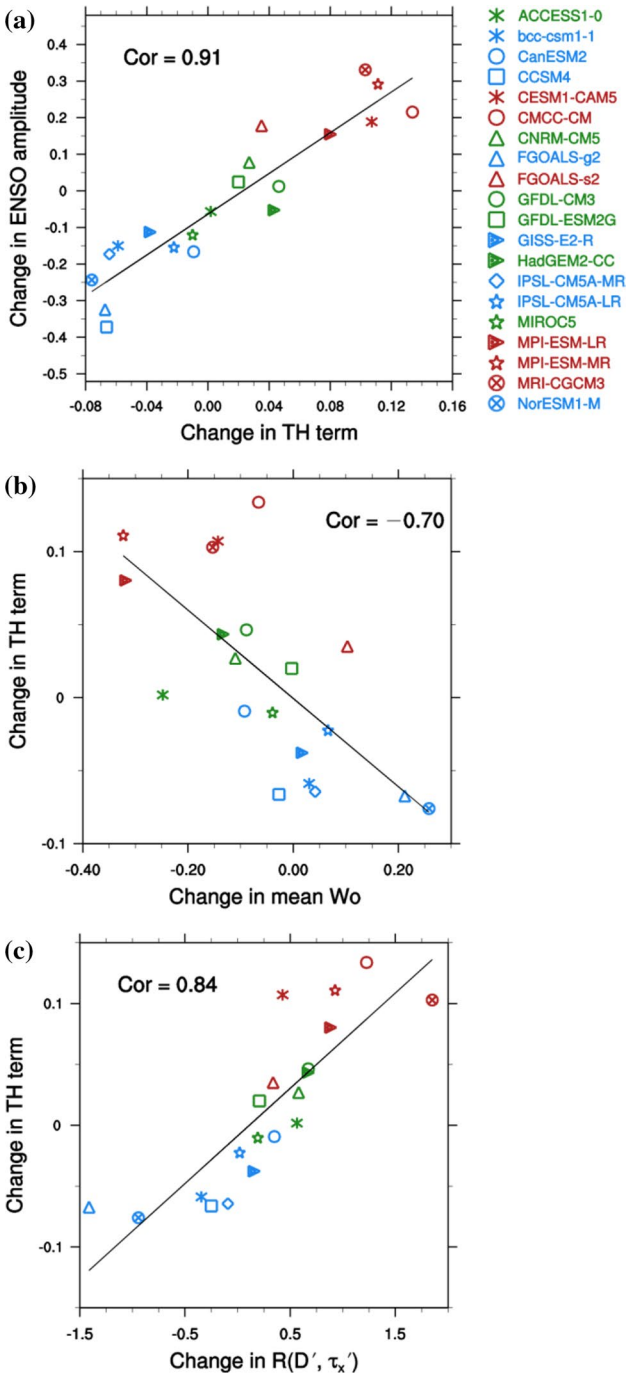

Fig. 2 **a** Scatter diagram showing relationship between ENSO amplitude change (K) and thermocline feedback change (K/month) derived from 20 CGCMs. **b** Scatter diagram showing relationship between thermocline feedback (TH) change (K/month) and the mean upwelling change (10^{-6} m/s) in the mixed layer over eastern equatorial Pacific (EEP). **c** Scatter diagram showing relationship between thermocline feedback change (K) and the change in the response of thermocline depth anomaly over Niño3 to the Niño4 zonal wind stress anomaly [i.e., $R(D', \tau_x')$, m/(N m^{-2})]. Labels in *red* (*blue*) denote the significantly strengthened (weakened) models, and the other labels in *green* denote the models with modest ENSO amplitude change

prompts us to concentrate on the change of perturbation part, which is associated with the three feedback coefficients in the right hand side of Eq. (4). By quantitatively examining the three feedback coefficients from each of the CMIP5 models, we found that the TH feedback change is primarily controlled by the change in $R(D', \tau_x')$, with a high correlation of 0.84 (Fig. 2c), whereas no significant correlation is found for $R(\tau_x', T')$ and $R(T_e', D')$. Therefore, the change of $R(D', \tau_x')$, i.e., the change of anomalous thermocline response to unit zonal wind stress anomaly in Niño4 (160°E–150°W, 5°S–5°N), holds a key for understanding divergent TH feedback changes under GW.

Next we separate 20 CMIP5 models into three groups, according to whether or not a model has a statistically significant increase or decrease of ENSO amplitude between GW and PD simulations with an F-test. We found that six models have a statistically significant strengthening of ENSO amplitude (named as ST group, indicated by the red check mark in Fig. 1a); eight models have a statistically significant weakening of ENSO amplitude (named as WK group, indicated by the blue check mark in Fig. 1a); the remaining models have modest ENSO amplitude change. Figure 3 shows the horizontal maps of composite $R(D', \tau_x')$ changes for the ST and WK models. As expected, the thermocline anomaly fields show that the response of anomalous thermocline over EEP to τ_x' increases in the ST group but decreases in the WK group under GW.

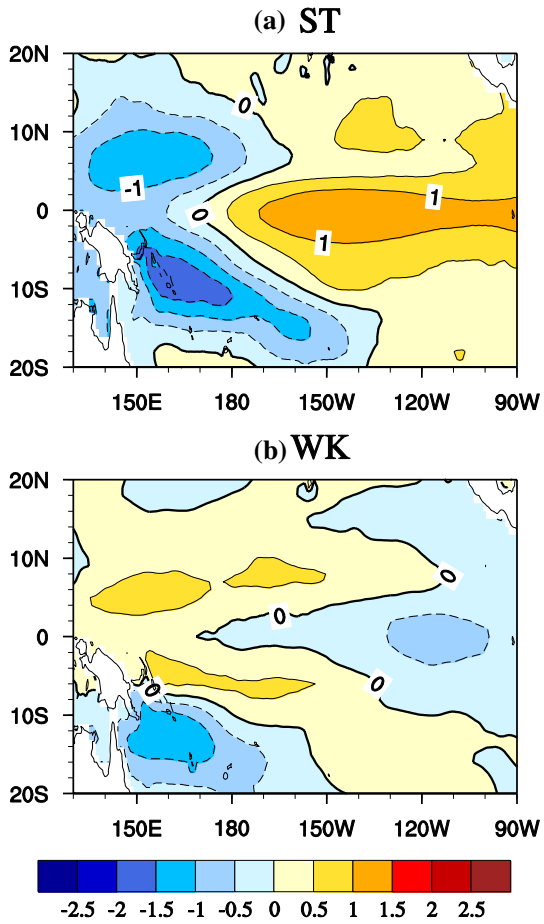

Fig. 3 Horizontal distribution of the composite thermocline response [i.e., $R(D', \tau_x')$] changes [GW minus PD; m/(N m^{-2})] under global warming for **a** ST models and **b** WK models

3.3 Analysis of changes in other air-sea feedbacks

It is of interest to notice that the ZA feedback $(-u'\frac{\partial \overline{T}}{\partial x})$ change is mainly attributable to the variation of anomalous zonal ocean flow (u'), not to the variation of mean zonal temperature gradient $(-\frac{\partial \overline{T}}{\partial x})$ (figure not shown). A further calculation (see Eq. 2–3) shows that u' is mainly controlled by geostrophic current (u_g') while Ekman current (u_e') has less contribution, which is in agreement with previous studies (Chen et al. 2015, Su et al. 2010, 2014). In ST/WK group, the change in D' over EEP maximizes/minimizes at the equator (Fig. 3a, b), corresponding to a positive/negative change in $-\partial^2 D'/\partial y^2$ and thus an increase/decrease in u_g' (see Eq. 2) . Therefore, the change of u' is primarily controlled by the change in D'. It is suggested that the contrasting changes in thermocline response [i.e., $R(D', \tau_x')$] hold a key for the contrasting changes of both TH and ZA feedbacks between the two groups.

The MA feedback $(-\overline{v}\frac{\partial T'}{\partial y})$ change is mainly controlled by the perturbation temperature gradient $(-\frac{\partial T'}{\partial y})$ change, which is due to the change of the SSTA and its meridional structure. The increase of SSTA magnitude as a result of the strengthened TH and ZA feedbacks could further

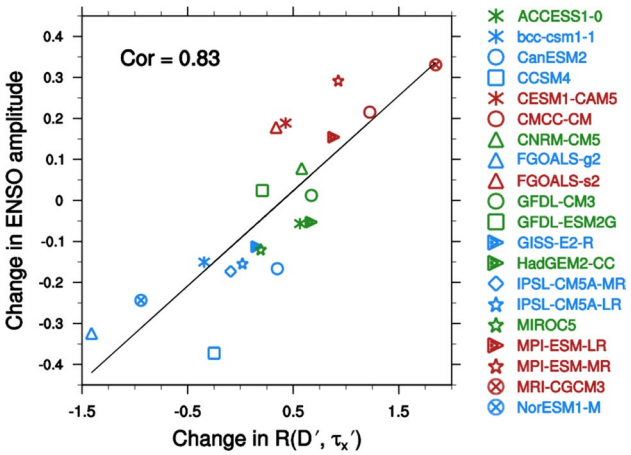

Fig. 4 Scatter diagram showing relationship between ENSO amplitude change (K) and the change in $R(D', \tau_x')$ [unit: m/(N m^{-2})]. Labels in *red* (*blue*) denote the significantly strengthened (weakened) models, and the other labels in *green* denote the models with modest ENSO amplitude change

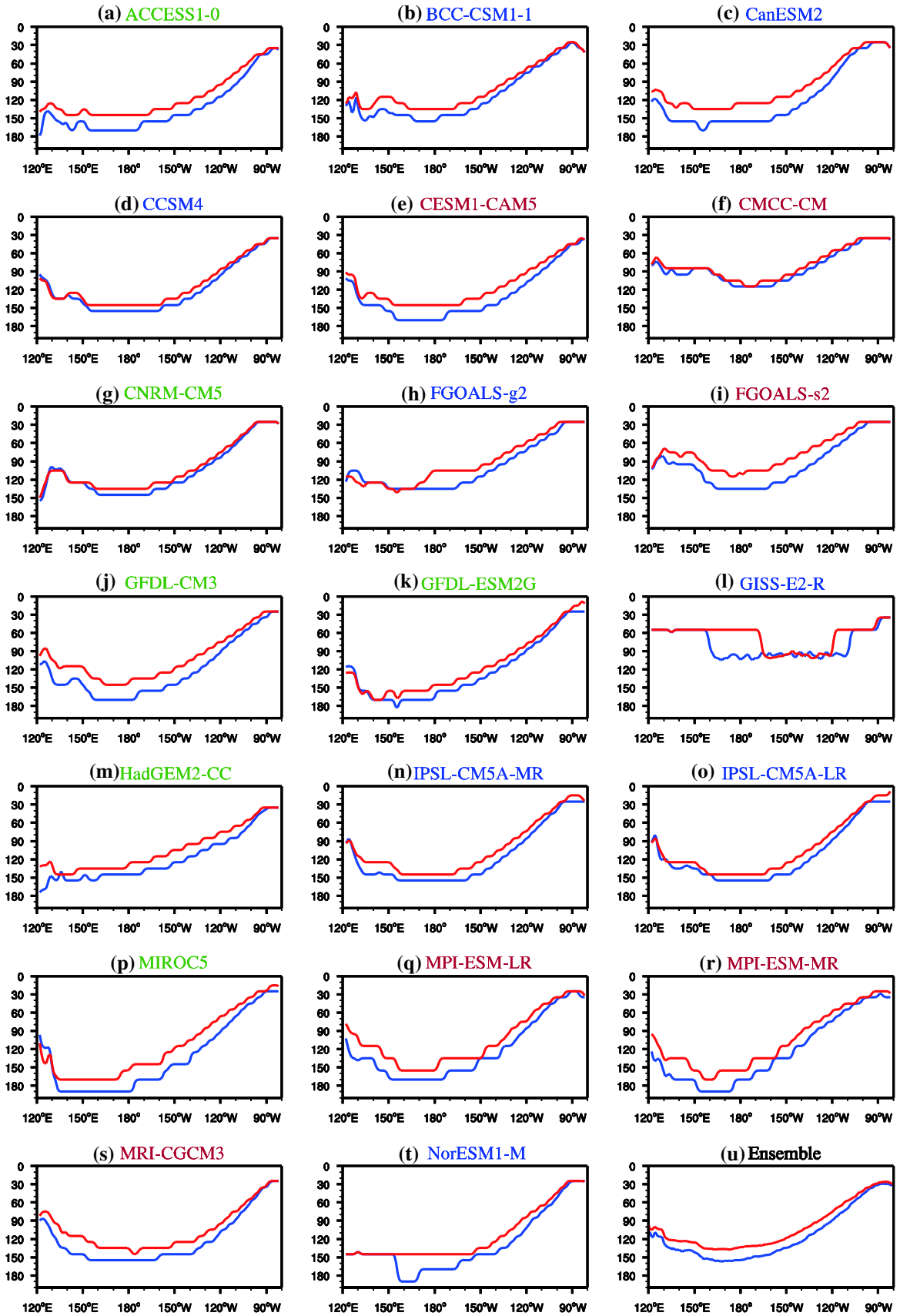
(a) ACCESS1-0
(b) BCC-CSM1-1
(c) CanESM2
(d) CCSM4
(e) CESM1-CAM5
(f) CMCC-CM
(g) CNRM-CM5
(h) FGOALS-g2
(i) FGOALS-s2
(j) GFDL-CM3
(k) GFDL-ESM2G
(l) GISS-E2-R
(m) HadGEM2-CC
(n) IPSL-CM5A-MR
(o) IPSL-CM5A-LR
(p) MIROC5
(q) MPI-ESM-LR
(r) MPI-ESM-MR
(s) MRI-CGCM3
(t) NorESM1-M
(u) Ensemble
0
30
60
90
120
150
180
120°E 150°E 180° 150°W 120°W 90°W

◂**Fig. 5** Mean thermocline depth in PD and GW. The *blue* and *red line* respectively indicate the mean thermocline depth in PD and GW for 20 CGCMs (**a**–**t**) and their multi-model ensemble mean (**u**). In both simulations, the mean thermocline depth is defined as the depth where the vertical gradient of mean temperature (averaged for 5°S–5°N) is maximum along the equator. Title in *red* (*blue*) denote the significantly strengthened (weakened) models, and the other titles with *green* denote the models with modest ENSO amplitude change

reinforce the MA feedback, because the climatological meridional surface current over EEP is generally poleward. On the other hand, the narrower (wider) meridional width of SSTA in ST (WK) models corresponds to stronger (weaker) $-\frac{\partial T'}{\partial y}$, which will be discussed in next section. The change of the EK feedback ($-w'\frac{\partial \overline{T}}{\partial z}$) is dominated by the change of perturbation vertical motion ($-w'$), which is linked with the change in zonal gradient of u' at the equator due to mass continuation. Because the maximum center of u' locates over the CEP and the u' becomes strengthened (weakened) in the ST (WK) models, the corresponding w' over EEP generally becomes strengthened (weakened), hence the anomalous upwelling feedback becomes strengthened (weakened) under GW.

The analysis above indicates that to the first order, the four feedback terms mentioned above are greatly affected by how the anomalous thermocline responds to unit zonal wind stress forcing in Niño4. This is confirmed by a high correlation (at a positive correlation of 0.83) between $R(D', \tau_x')$ change and ENSO amplitude change among the 20 CMIP5 models (Fig. 4). Thus, the change in the thermocline response [i.e., $R(D', \tau_x')$] can be regarded as a key factor that determines the ENSO amplitude change under GW.

4 What determines the divergent changes in thermocline response?

An interesting issue is what causes the divergent changes in thermocline response over EEP among the CMIP5 models, given the same unit τ_x' forcing in Niño4. Based on the Sverdrup balance (Jin 1997; Neelin 1991), the relationship between the equatorial τ_x' and D' may be written as below:

$$\frac{\partial D'}{\partial x} = \frac{\tau_x'}{\rho_o g H_1}, \tag{5}$$

in which H_1 represents the climatological thermocline depth.

According to Eq. (5), two factors may influence the anomalous thermocline tilting at the equator. One is the mean thermocline depth change, and the other is the change in the strength of τ_x' at the equator. We first examine whether there is a contrasting change in the climatological equatorial thermocline depth under GW. It's found that the climatological thermocline in the equatorial Pacific becomes shallow in all the CMIP5 models (Fig. 5). Such a common feature is in agreement with the CMIP3 results reported by pervious study (Yeh et al. 2009). The consensus on the change of the mean thermocline depth cannot explain the contrasting thermocline responses between ST and WK groups.

In the following we examine if a contrasting change exists in the strength of τ_x' at the equator between ST and WK groups. Figure 6 shows the meridional sections of τ_x' averaged over CEP, which were derived from the regression against time series of Niño4 τ_x'. Note that the meridional structure of τ_x' becomes wider and flatter in the WK group but narrower and sharper in the ST group under GW. This indicates that τ_x' strengthens (weakens) at the equator in the ST (WK) group under GW, given the same box-averaged τ_x' forcing in Niño4. A strengthened (weakened) τ_x' at the equator can induce a greater (smaller) thermocline response over EEP, based on Eq. (5).

With respect to the change in meridional structure of τ_x', one may quantitatively measure the meridional width of τ_x' with a width index. The meridional width index (hereafter *WI*) is defined using the following formula (Merryfield 2006; Chen et al. 2015):

$$WI = \frac{\int_{5S}^{5N} X(y) \cdot |y| \, dy}{\int_{5S}^{5N} X(y) \, dy} \tag{6}$$

where $X(y)$ represents the value of a certain field (e.g., τ_x') at the latitude of y. We calculated the *WI* of the regressed τ_x' field averaged over 160°E–150°W (as shown in Fig. 6a, b), for both PD and GW simulations derived from each model. Our calculation shows that the changes in the *WI* of τ_x' are highly negatively correlated with the change in $R(D', \tau_x')$, with a correlation coefficient of −0.85 (Fig. 7). This implies that when ENSO-related τ_x' field becomes more (less) confined to the equator (i.e., smaller (greater) *WI*), τ_x' is strengthened (weakened) at the equator and it thus promotes anomalous thermocline response over EEP more (less) effectively, given the same unit of τ_x' forcing over Niño4 region.

The meridional structure change of τ_x' is consistent with the meridional width change of SSTA. Figure 8 show the meridional structures of the normalized standard deviation of SSTA averaged over 150°W–90°W. The meridional profile of SSTA in the ST (WK) group turns sharper (flatter) in GW compared to PD, matching well with the change in τ_x'. Thus, as a coupled system, ENSO experiences a consistent meridional structure change in both the zonal wind stress and SST anomalies under GW.

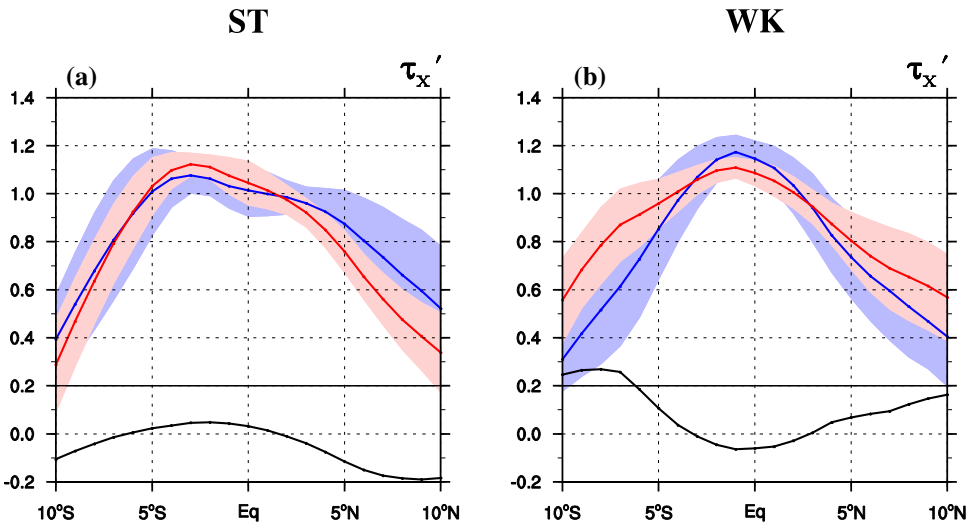

Fig. 6 Changes in the meridional structures of τ_x' from PD (*blue*) to GW (*red*). Meridional structures of the regressed τ_x' averaged over 160°E–150°W [units: N m^{-2}/(N m^{-2})], derived from composite (**a**) ST and (**b**) WK models. The regressed τ_x' is obtained by regressing τ_x' onto Niño4 τ_x' [units: N m^{-2}/(N m^{-2})]. The *blue line* and *red line* respectively represent the PD and GW simulations, the *black line* indicates the difference (GW minus PD), the *light blue shading* and the *light red shading* indicate inter-model spread, which is estimated with the inter-model standard deviations in the PD and GW simulations, respectively

5 Cause of ENSO meridional structure changes

Previous studies (Zhang et al. 2009, 2013b; Zhang and Jin 2012) suggested that the climatologic mean meridional current is critical in controlling the ENSO meridional scale. Figure 9 illustrates the change of the mean meridional currents associated with the Pacific subtropical cell (McCreary and Lu 1994; hereafter STC) in the tropical Pacific. The mean surface poleward meridional current becomes weaker in ST (Fig. 9a) but stronger in WK (Fig. 9b), so does the STC. A t-test shows that the difference in the changes of climatological STC strength between the ST and WK groups are significant (Fig. 9c). Physically, it is argued that a strengthened (weakened) mean surface poleward meridional current leads to a flatter but wider (sharper but narrower) ENSO width, through the mean flow advective effect. Such argument is supported by the model diagnosis. Indeed, a strengthened (weakened) climatologic mean STC in the WK (ST) group generally corresponds to a widened (narrowed) SSTA and τ_x' in meridional direction under GW.

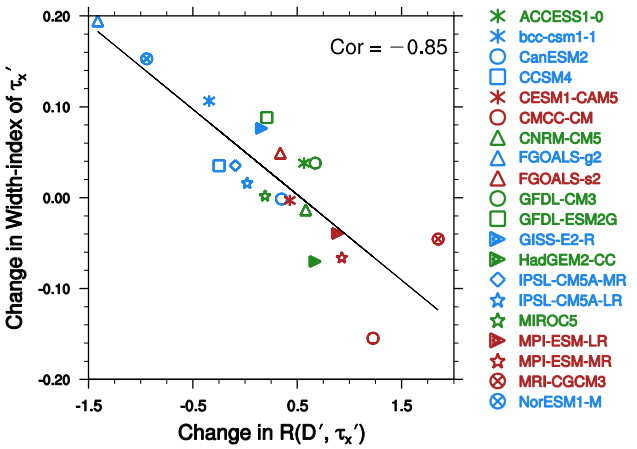

Fig. 7 Scatter diagram showing relationship between the change in meridional structure of τ_x' (unit: degree of latitude) and the change in thermocline response [unit: m/(N m^{-2})]. Here the change in the width index of the regressed τ_x' field averaged over Niño4 longitudinal range 160°E–150°W (which is obtained from the results as shown in Fig. 6), is applied to measure the meridional structure change

6 How would STC change under GW?

The above step-by-step diagnosis result indicates that the change of future ENSO intensity depends greatly on how the mean STC changes. Figure 10 illustrates the inter-model relationship between ENSO amplitude change and the change in the mean surface meridional current. As expected, a strengthened (weakened) mean surface poleward current generally corresponds to a weakened (strengthened) ENSO amplitude under GW. Based on this reversed relationship between ENSO amplitude change and mean STC change, then a key issue is how the climatological STC would change under GW.

Despite of divergent ENSO projection, it is reported that most CMIP5 models projected a robust zonal mean SST change under GW, with a much greater polar warming

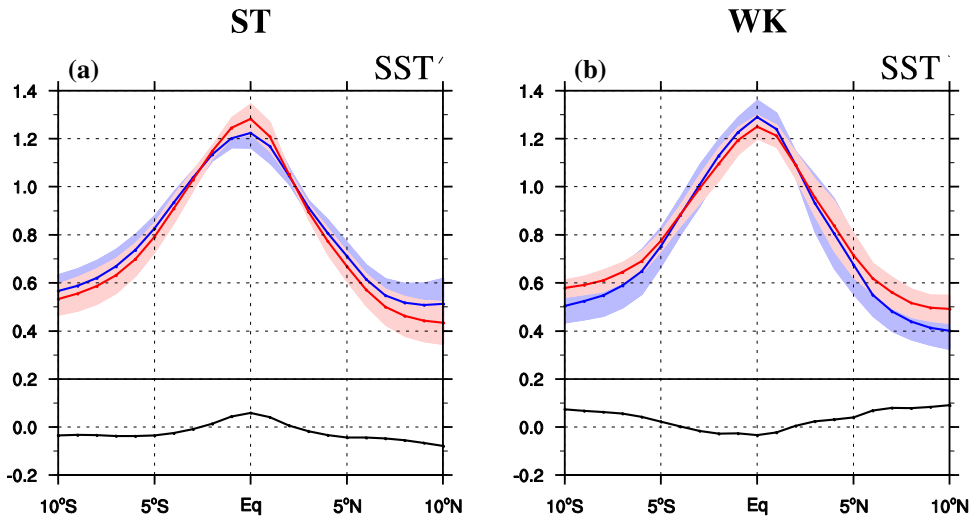

Fig. 8 Changes in the meridional structures of SSTA from PD (*blue*) to GW (*red*). Meridional structures of the normalized SSTA STD averaged over 150°W–90°W (units: K/K), derived from the composite (**a**) ST and (**b**) WK models. The *blue line* and *red line* respectively represent the PD and GW simulations, the *black line* indicates the difference (GW minus PD), the *light blue shading* and the *light red shading* indicate inter-model spread, which is estimated with the inter-model standard deviations in the PD and GW simulations, respectively

than a weaker warming in tropics (Fig. 11a, or see Fig. 1b in Zhang and Li 2014, hereafter ZL 2014). The physical cause of this robust zonal mean SST change projection arises from a longwave radiation—evaporation damping mechanism (see Xie et al. 2010; ZL 2014). As demonstrated by ZL (2014) (see their Fig. 2), because of this mechanism, the future change of the mean SST field is, to the large extent, controlled by the present-day mean SST pattern. This is why most CMIP5 models project a robust zonal mean SST change despite of uncertainty in interannual variability. Based on this robust feature, we tried to explore theoretically how the zonal mean surface wind would change, in response to the robust zonal mean SST change. Specifically, we employed a simple theoretical model (Lindzen and Nigam 1987; Wang and Li 1993) to estimate the change of zonally-averaged mean zonal wind stress (i.e., $\delta[\tau_x]$). Here δ means the difference between GW and PD, and "[]" represents the zonal (0°–360°E) average. The equations for this simple theoretical model and detailed derivation procedure are provided in the Appendix. Forced by the multi-model ensemble (MME) average of the zonally-averaged mean SST change (i.e., δ[SST], as shown in Fig. 11a), the theoretical model projects the meridional profile of $\delta[\tau_x]$, as shown in Fig. 11b. This theoretical estimation resembles that derived from CMIP5 MME average (Fig. 11c), with a pattern correlation of 0.58 in the tropics (30°S–30°N).

Our next strategy is to force an OGCM with the theoretically estimated $\delta[\tau_x]$ to investigate how the mean STC would change. In a control run, the OGCM is driven by the observed climatological wind stress field. In the sensitivity run, the projected $\delta[\tau_x]$ is added to the climatological wind stress field. The difference of simulated STC fields between the sensitivity and control runs indicates the estimation of the future STC change in response to $\delta[\tau_x]$. The OGCM simulation shows that the Pacific STC is weakened in response to the theoretically derived $\delta[\tau_x]$ (Fig. 12). Given the reversed relationship between the ENSO amplitude change and the mean STC change derived from 20 CMIP5 models, it is speculated that the future ENSO amplitude would increase.

7 Summary and discussion

This study provides a possible explanation of why CMIP5 models generate divergent ENSO projections under GW. Through careful examination of the mixed-layer heat budget for each of the models, we unveil key physical processes behind this diversity. In particular, through a step-by-step approach, we addressed the following key science questions: (1) given a number of positive and negative feedbacks involved during the ENSO development, which feedback process is crucial in causing the divergent ENSO projections? Our mixed-layer heat budget results reveal that it mainly lies in the TH feedback change; (2) given that the change of TH feedback involves both the perturbation change and the mean state change, which is of major cause? Our analysis shows that it primarily arises from the perturbation change; (3) as the TH feedback involves atmospheric wind response to SSTA, ocean thermocline response to wind anomaly, and ocean subsurface temperature response to thermocline anomaly, which of the above processes is critical? Our result shows that it is primarily due to the ocean thermocline response to wind forcing (i.e., $R(D', \tau_x')$); (4) given a unit wind stress forcing over Niño4 box, what causes the contrasting changes of $R(D', \tau_x')$ among CMIP5 models? The answer is that it is attributable to the contrasting change of ENSO meridional structure, which is further shown to be controlled by the change of mean STC; (5) how would the STC change under GW? Our strategy is first to project the zonally-averaged mean zonal wind stress

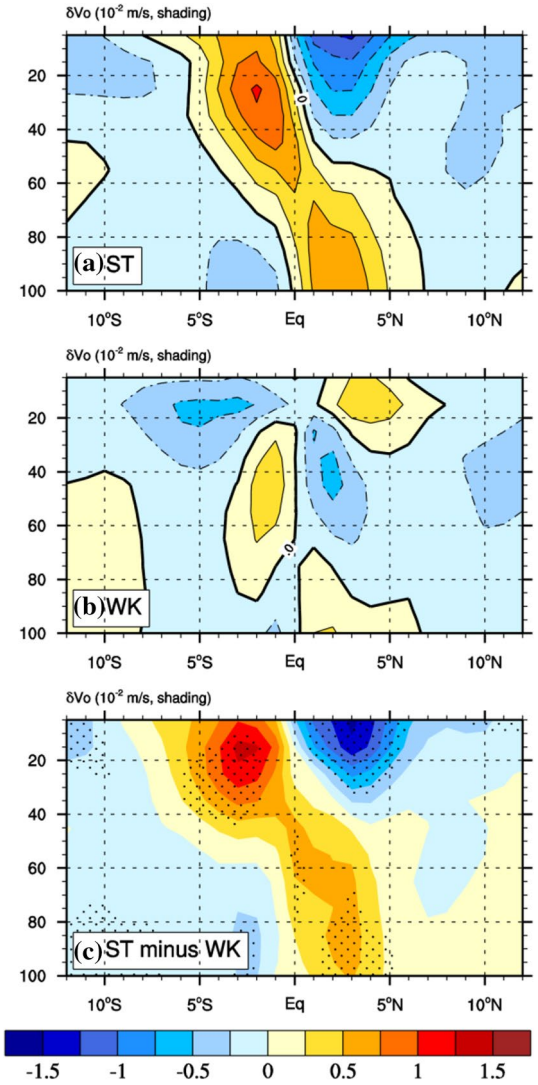

Fig. 9 Composite change in climatological meridional ocean current (δV_o, 10^{-2} m/s) averaged over 160°E–90°W derived from **a** ST and **b** WK models, as well as **c** their difference (ST minus WK). The stippling in **c** indicates the difference between ST and WK exceeding a confidence level of 95% using Student's *t* test

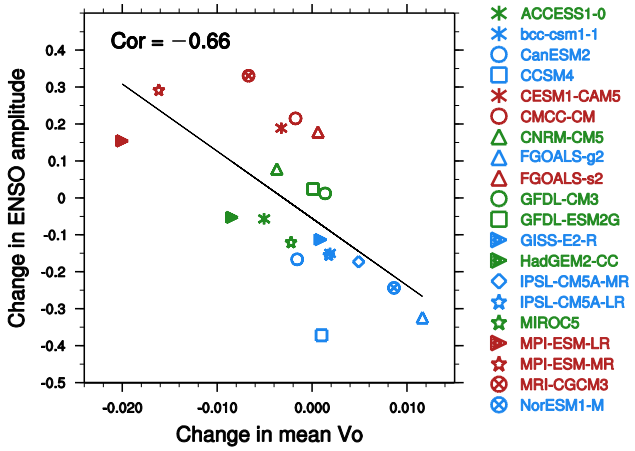

Fig. 10 Scatter diagram showing relationship between the ENSO amplitude change (unit: K) and the change in the mean surface poleward meridional current (unit: m s^{-1}; averaged for 160°E–90°W, 5°S–5°N and 0–30 m) among CMIP5 models. When calculating the change in mean meridional current, the value in the Southern Hemisphere was multiplied by −1. Labels in *red* (*blue*) denote the significantly strengthened (weakened) models, and the other labels in *green* denote the models with modest ENSO amplitude change

change based on the robust zonally-averaged mean SST change pattern among the CMIP5 models, and then to force an OGCM with the theoretically estimated mean zonal wind stress change field to estimate the mean STC change.

As analyzed above, the ENSO amplitude projections are divergent among the 20 CMIP5 models. The CMIP5-ensemble average of ENSO amplitude change is nearly zero, and so is that of the mean STC change. However, by examining individual model results, one could find a significant increase or decrease of ENSO amplitude. This prompts us to understand the cause of the divergent changes among the models, as the first step. The main conclusion derived from the model diagnosis is that there is a statistically significant relationship between the ENSO amplitude change and the mean STC change among these models. The next step is to project future mean STC change. Here we attempted to develop a theoretical approach to estimate the future mean STC change. Such a new strategy, at least, represents a new alternative for addressing the future ENSO projection problem.

Based on the argument of robustness of mean state change (Xie et al. 2010; ZL 2014) and the chains of causation between the ENSO amplitude change and the mean STC change derived in the current study, we speculated that the future ENSO amplitude would increase. This projection appears consistent with increased frequencies of extreme El Niño and extreme La Niña, reported by Cai et al. (2014, 2015b), and the implication from a palaeoclimate study (Sadekov 2013). It is worth mentioning that the current projection of ENSO amplitude increase is built based on the model world. A further study to reduce the uncertainty of future ENSO projection is still needed.

One may question that whether the modulation of ENSO amplitude would further rectify the mean state (e.g., mean STC), which could in turn regulate the interannual variability. The ENSO variability involves both positive (El Niño) and negative (La Niña) events. Linear effects of combination of anomalous downwelling/upwelling from strengthened (or weakened) El Niño/La Niña events will be canceled out,

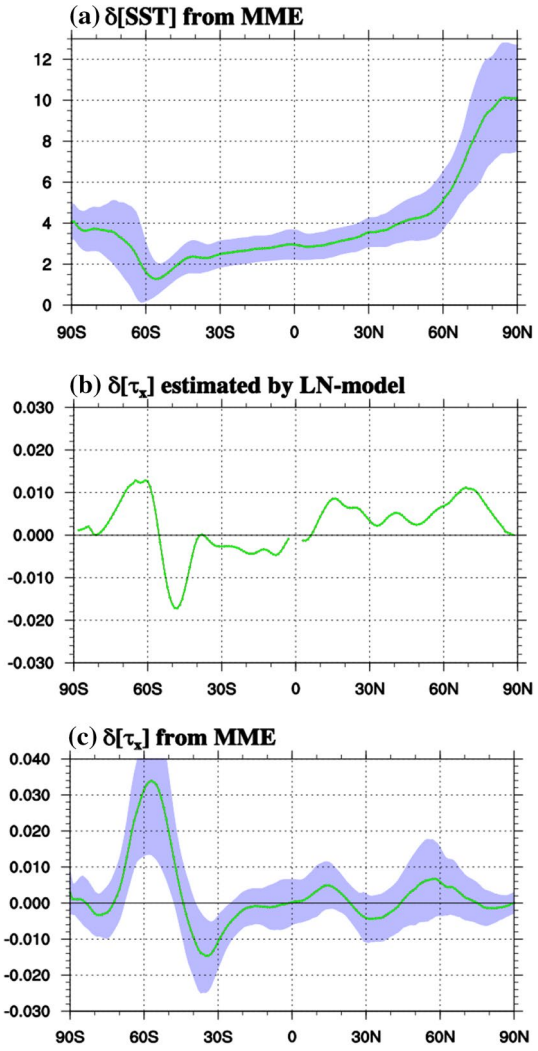

Fig. 11 Projected changes of zonally-averaged mean SST and mean zonal wind stress. **a** *Green line* denotes the change of zonally-averaged (0°–360°E) mean SST (i.e., δ[SST]; units: K) derived from CMIP5 MME average, and shading indicates inter-model spread, which is estimated based on the inter-model standard deviation. **b** *Green line* is the change of the zonally-averaged mean zonal wind stress (i.e., $\delta[\tau_x]$; unit: N m^{-2}), which is estimated by the simple theoretical model. The value is not plotted within 2°S–2°N, where it approaches infinity. **c** Same as **a** except for the $\delta[\tau_x]$ (unit: N m^{-2}) derived from CMIP5 MME average

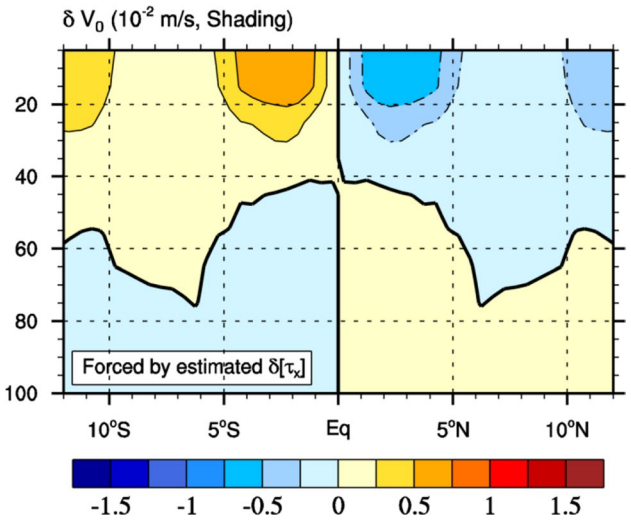

Fig. 12 The change of climatological meridional current (*shading*; 10^{-2} m s^{-1}) averaged over 160°E–90°W, which is obtained by forcing an OGCM with a theoretically estimated $\delta[\tau_x]$ (as shown in Fig. 11b)

and only nonlinear rectification effect accounts for the mean state change. Study of such an upscale feedback process is in general quite complicated. Study of the mean state impact on perturbations (such as ENSO-related interannual variability), on the other hand, is more simple and straight-forward. How the climate would respond to GW is to large extent an issue associated with the change in external forcing. To the first order, one may examine how the mean state responds to the increase of greenhouse gases such as CO_2. Therefore, a direct approach is first to reveal how the mean state changes, and then to examine how the mean state change further affects the perturbation. The next step will be to examine how the altered perturbation further feeds back to the mean state. This upscale feedback part will be investigated in our future work.

Acknowledgements We would like to thank Dr. Lu Wang and anonymous reviewers for insightful suggestions and comments. We acknowledge the PCMDI for providing the CMIP5 model data, which may be obtained from the website of http://pcmdi9.llnl.gov/esgf-web-fe/. This work was supported by NSFC project 41630423, National 973 project 2015CB453200, NSF AGS-1565653, NSFC 41475084, NRL grant N00173-161G906, Jiangsu NSF project BK20150062, Jiangsu Shuang-Chuang Team (R2014SCT001), NSFC Grant 41376002/41606011/41530426, CAS Strategic Priority Project XDA11010105, and by the IPRC that is sponsored by Japan Agency for Marine-Earth Science and Technology (JAMSTEC). This is SOEST contribution number 9938, IPRC contribution number 1237, and ESMC contribution 150.

Appendix: A simple theoretical model

Based on a simplified Lindzen–Nigam model (Lindzen and Nigam 1987; Wang and Li 1993), boundary-layer zonal and meridional wind fields may be written as:

$$Eu - fv = A\frac{\partial T}{\partial x} \tag{7}$$

$$Ev + fu = A\frac{\partial T}{\partial y} \tag{8}$$

in which u (v) denotes the mean zonal (meridional) wind field averaged in the boundary layer, T denotes the mean sea surface temperature, f represents the Coriolis parameter, E represents the frictional coefficient (10^{-5} s^{-1}),

$A = R\frac{p_s - p_e}{2p_e}$ is the SST-gradient forcing coefficient, R is the gas constant for dry air (287 J K^{-1} kg^{-1}), p_e denotes the pressure at top of the boundary layer (850 hPa), and p_s denotes the pressure at bottom of the boundary layer (1000 hPa).

Applying a zonal (0°–360°E) average operator to Eqs. (7, 8), we have

$$E[u] - f[v] = 0 \tag{9}$$

$$E[v] + f[u] = A\frac{\partial[T]}{\partial y} \tag{10}$$

where "[]" represents the zonal average. Thus, we can obtain

$$[u] = A\frac{\partial[T]}{\partial y}/(\frac{E^2}{f} + f) \tag{11}$$

Assuming coefficients A and E are constant in the present-day and future global warming climate states, one may obtain

$$\delta[u] = A\frac{\partial\delta[T]}{\partial y}/\left(\frac{E^2}{f} + f\right) \tag{12}$$

where δ means the future changes (using GW minus PD).

The change of zonally-averaged mean zonal wind stress (i.e., $\delta[\tau_x]$) may be determined by the following equation

$$\delta[\tau_x] = \rho_a C_D\left|\vec{V}\right|\delta[u] = \rho_a C_D\left|\vec{V}\right|A\frac{\partial\delta[T]}{\partial y}/\left(\frac{E^2}{f} + f\right) \tag{13}$$

where τ_x denotes the mean zonal wind stress field, ρ_a denotes the atmosphere density (1.29 kg m^{-3}), C_D denotes the drag coefficient (1.5×10^{-3}), and $\left|\vec{V}\right|$ denotes the surface wind speed in PD.

References

Ashok K, Behera SK, Rao SA, Weng H, Yamagata T (2007) El Niño Modoki and its possible teleconnection. J Geophys Res 112. doi:10.1029/2006JC003798

Cai W et al (2014) Increasing frequency of extreme El Nino events due to greenhouse warming. Nat Clim Change 4:111–116

Cai W et al (2015a) ENSO and greenhouse warming. Nature Clim Change 5:849–859 doi:10.1038/nclimate2743

Cai W et al (2015b) Increased frequency of extreme La Niña events under greenhouse warming. Nat Clim Change 5:132–137

Chang P, Philander SG (1994) A coupled ocean-atmosphere instability of relevance to the seasonal cycle. J Atmos Sci 51:3627–3648

Chen L, Li T, Yu Y (2015) Causes of strengthening and weakening of ENSO amplitude under global warming in four CMIP5 models. J Clim 28:3250–3274. doi:10.1175/jcli-d-14-00439.1

Chung P-H, Li T (2013) Interdecadal relationship between the mean state and El Niño Types*. J Clim 26:361–379

Collins M et al (2010) The impact of global warming on the tropical Pacific Ocean and El Niño. Nature Geosci 3:391–397

DiNezio PN, Clement AC, Vecchi GA, Soden BJ, Kirtman BP, Lee S-K (2009) Climate response of the equatorial Pacific to global warming. J Clim 22:4873–4892

Ding R, Li JP (2012) Influences of ENSO teleconnection on the persistence of sea surface temperature in the Tropical Indian Ocean. J Clim 25:8177–8195. doi:10.1175/JCLI-D-11-00739.1

Feng J, Li JP (2011) Influence of El Niño Modoki on spring rainfall over south China. J Geophys Res Atmos 116:D13102. doi:10.1029/2010jd015160

Feng J, Li JP (2013) Contrasting impacts of two types of ENSO on the boreal spring Hadley circulation. J Clim 26:4773–4789. doi:10.1175/JCLI-D-12-00298.1

Feng J, Li J, Zhu J, Liao H (2016) Influences of El Niño Modoki event 1994/1995 on aerosol concentrations over southern China. J Geophys Res Atmos 121:2015JD023659. doi:10.1002/2015jd023659

Guilyardi E et al (2009) Understanding El Nino in ocean–atmosphere general circulation models. Bull Amer Meteor Soc 90:325–340

Ham Y-G, Kug J-S (2016) ENSO amplitude changes due to greenhouse warming in CMIP5: Role of mean tropical precipitation in the twentieth century. Geophys Res Lett 43. doi:10.1002/2015gl066864

Jin F-F (1997) An equatorial ocean recharge paradigm for ENSO. Part I: conceptual model. J Atmos Sci 54:811–829

Kao HY, Yu JY (2009) Contrasting eastern-Pacific and central-Pacific types of ENSO. J Clim 22:615–632

Karori MA, Li JP, Jin F-F (2013) The asymmetric influence of the two types of El Niño and La Niña on summer rainfall over Southeast China. J Clim 26:4567–4582. doi:10.1175/JCLI-D-12-00324.1

Kim ST, Cai W, Jin F-F, Santoso A, Wu L, Guilyardi E, An S-I (2014) Response of El Nino sea surface temperature variability to greenhouse warming. Nat Clim Change 4:786–790 doi:10.1038/nclimate2326

Kug JS, Jin FF, An SI (2009) Two types of El Niño events: cold tongue El Niño and warm pool El Niño. J Clim 22:1499–1515

Larkin NK, Harrison DE (2005) On the definition of El Niño and associated seasonal average US weather anomalies. Geophys Res Lett 32:L13705. doi:10.1029/2005gl022738

Latif M, Keenlyside N (2009) El Niño/Southern Oscillation response to global warming. Proc Natl Acad Sci 106:20578–20583

Li T (1997) Phase transition of the El Niño-southern oscillation: a stationary SST mode. J Atmos Sci 54:2872–2887

Li T, Zhang Y, Lu E, Wang D (2002) Relative role of dynamic and thermodynamic processes in the development of the Indian Ocean dipole: an OGCM diagnosis. Geophys Res Lett 29:25-21-25-24

Lindzen RS, Nigam S (1987) On the role of sea surface temperature gradients in forcing low-level winds and convergence in the tropics. J Atmos Sci 44:2418–2436

Liu L, Yu W, Li T (2011) Dynamic and thermodynamic air–sea coupling associated with the Indian Ocean dipole diagnosed from 23 WCRP CMIP3 models*. J Clim 24:4941–4958

Liu H, Lin P, Yu Y, Zhang X (2012) The baseline evaluation of LASG/IAP climate system ocean model (LICOM) version 2. Acta Meteorol Sin 26:318–329

McCreary JP Jr, Lu P (1994) Interaction between the subtropical and equatorial ocean circulations: the subtropical cell. J Phys Oceanogr 24:466–497

McPhaden MJ, Zebiak SE, Glantz MH (2006) ENSO as an integrating concept in earth science. Science 314:1740–1745. doi:10.1126/science.1132588

Merryfield WJ (2006) Changes to ENSO under CO_2 doubling in a multimodel ensemble. J Clim 19:4009–4027

Neelin JD (1991) The slow sea surface temperature mode and the fast-wave limit: analytic theory for tropical interannual

oscillations and experiments in a hybrid coupled model. J Atmos Sci 48:584–606

Philander SG (1990) El Niño, La Niña, and the southern oscillation. Academic Press, London

Power S, Delage F, Chung C, Kociuba G, Keay K (2013) Robust twenty-first-century projections of El[thinsp]Nino and related precipitation variability. Nature 502:541–545. doi:10.1038/nature12580

Rashid HA, Hirst AC, Marsland SJ (2016) An atmospheric mechanism for ENSO amplitude changes under an abrupt quadrupling of CO_2 concentration in CMIP5 models. Geophys Res Lett 43:2015GL066768. doi:10.1002/2015gl066768

Sadekov AY, Ganeshram R, Pichevin L, Berdin R, McClymont E, Elderfield H, Tudhope AW (2013) Palaeoclimate reconstructions reveal a strong link between El Nino-Southern Oscillation and Tropical Pacific mean state. Nat Commun 4 doi:10.1038/ncomms3692

Stevenson SL (2012) Significant changes to ENSO strength and impacts in the twenty-first century: Results from CMIP5. Geophys Res Lett 39:L17703. doi:10.1029/2012gl052759

Su J, Zhang R, Li T, Rong X, Kug J, Hong C-C (2010) Causes of the El Niño and La Niña amplitude asymmetry in the equatorial eastern Pacific. J Clim 23:605–617

Su J, Li T, Zhang R (2014) The initiation and developing mechanisms of central Pacific El Niños. J Clim 27:4473–4485

Taylor KE, Stouffer RJ, Meehl GA (2012) An overview of CMIP5 and the experiment design. Bull Am Meteorol Soc 93:485

Van Oldenborgh GJ, Philip S, Collins M (2005) El Niño in a changing climate: A multi-model study. Ocean Sci Discuss 1:81–95

Wang B, Li T (1993) A simple tropical atmosphere model of relevance to short-term climate variations. J Atmos Sci 50:260–284

Wang C, Weisberg RH (1994) On the "Slow Mode" mechanism in ENSO-related coupled ocean–atmosphere models. J Climate 7:1657–1667

Xiang B, Wang B, Li T (2013) A new paradigm for the predominance of standing Central Pacific Warming after the late 1990s. Clim Dyn 41:327–340

Xie SP, Deser C, Vecchi GA, Ma J, Teng H, Wittenberg AT (2010) Global warming pattern formation: sea surface temperature and rainfall*. J Clim 23:966–986

Yeh S-W, Kirtman BP (2007) ENSO amplitude changes due to climate change projections in different coupled models. J Clim 20:203–217

Yeh SW, Kug JS, Dewitte B, Kwon MH, Kirtman BP, Jin FF (2009) El Niño in a changing climate. Nature 461:511–514

Zelle H, van Oldenborgh GJ, Burgers G, Dijkstra H (2005) El Niño and greenhouse warming: results from ensemble simulations with the NCAR CCSM. J Clim 18:4669–4683

Zhang W, Jin F-F (2012) Improvements in the CMIP5 simulations of ENSO-SSTA meridional width. Geophys Res Lett. doi:10.1029/2012GL053588

Zhang L, Li T (2014) A simple analytical model for understanding the formation of sea surface temperature patterns under global warming. J Clim 27:8413–8421. doi:10.1175/jcli-d-14-00346.1

Zhang W, Li J, Jin FF (2009) Spatial and temporal features of ENSO meridional scales. Geophys Res Lett 36. doi:10.1029/2009GL038672

Zhang W, Jin F-F, Zhao J-X, Qi L, Ren H-L (2013a) The possible influence of a nonconventional El Niño on the severe autumn drought of 2009 in Southwest China. J Clim 26:8392–8405. doi:10.1175/JCLI-D-12-00851.1

Zhang W, Jin F-F, Zhao J-X, Li J (2013b) On the bias in simulated ENSO SSTA meridional widths of CMIP3 models. J Clim 26:3173–3186